

# The structure of the $X(3915)$ meson and its production in heavy ion collisions

Sungtae Cho,<sup>1,\*</sup> Aaron Park,<sup>2,†</sup> Su Houn Lee,<sup>2,‡</sup> and Sungsik Noh<sup>1,§</sup>

<sup>1</sup>*Division of Science Education, Kangwon National University, Chuncheon 24341, Korea*

<sup>2</sup>*Department of Physics and Institute of Physics and Applied Physics, Yonsei University, Seoul 03722, Korea*

We study the structure of the  $X(3915)$  meson in a quark model and explore how its production in heavy ion collisions depends on its internal structure. We first analyze the  $X(3915)$  as a  $c\bar{c}ss\bar{s}$  state and solve the Hamiltonian with color-spin interactions within the quark model. We find that the ground state of the  $c\bar{c}ss\bar{s}$  with total spin 0 obtained from the quark model analysis favors a separated  $D_s\bar{D}_s$  state. To probe its structure further, we study its production in relativistic heavy ion collisions for various proposed configurations. We calculate the transverse momentum distributions and yields for the  $X(3915)$  assuming its structure to be either a charmonium, a tetraquark, or a hadronic molecular state. We argue that by measuring the transverse momentum distributions and yields of the  $X(3915)$  produced in heavy ion collisions, one can identify the structure of the  $X(3915)$ .

## I. INTRODUCTION

Since the  $X(3872)$  meson was observed in 2003 by the Belle Collaboration [1], many new hadrons with the names  $X$ ,  $Y$  and  $Z$  have been observed [2–4]. The  $X(3915)$  meson discovered by the Belle Collaboration in 2004 [5] from the analysis of the  $\omega J/\psi$  invariant mass in the  $B$  meson decay is one of those  $XYZ$  hadrons. The  $X(3915)$  has also been observed by the BaBar Collaboration [6, 7], and its quantum number could be determined as  $I^G(J^{PC}) = 0^+(0^{++})$  by the Belle Collaboration and subsequently confirmed by the BaBar Collaboration [8, 9]. As a result, it is listed and renamed in the Particle Data Group as the  $\chi_{c0}(3915)$  [10].

The mass of the  $X(3915)$  meson is close to that of the  $X(3872)$ , but the two states differ significantly in their properties. The  $X(3915)$  has quantum numbers  $0^+(0^{++})$ , in contrast to the  $X(3872)$ , which has  $0^+(1^{++})$ . Unlike the  $X(3872)$ , which decays dominantly into  $\bar{D}^* D^0$ , the  $X(3915)$  lies below the  $D_s\bar{D}_s$  threshold but is considered capable of decaying into these mesons, analogous to the  $X(3960)$  recently observed by LHCb Collaboration [11], and possibly having strange quarks as its constituents.

Like most  $XYZ$  hadrons including the  $X(3872)$  meson, the internal structure of the  $X(3915)$  meson has not been clearly understood to date, and the proposed structures of the  $X(3915)$  include an  $s$ -wave molecular bound state of the  $D_s\bar{D}_s$  pair [12], a compact  $c\bar{c}ss\bar{s}$  tetraquark state [13], a conventional  $c\bar{c}$  state [14], and a hadronic molecular state with the probability of a bare  $c\bar{c}$  state less than 45% [15].

Regarding the  $X(3872)$ , there have been attempts to understand the structure of the  $X(3872)$  [16–18], including studies in the quark model [19] and in heavy ion collisions [20–22]. Moreover, there have also been

general studies on the possibilities of the bound state of exotic hadrons composed of four quarks, in various combinations in the quark model with color-spin interactions, focusing on doubly heavy exotic hadrons such as  $T_{cc}$  [23–26]. These studies have significantly advanced our understanding of multiquark states in open heavy flavor sectors. However, despite these extensive efforts, the internal structure of hidden charm and hidden strangeness tetraquarks with  $c\bar{c}ss\bar{s}$  configuration remains much less well understood than that of open heavy flavor tetraquarks. In particular, the calculation in Ref. [27] was limited to the color-spin interaction only. The authors of Ref. [28] employed a full model Hamiltonian, however, their predicted mass for the  $c\bar{c}ss\bar{s}$  configuration does not reproduce the experimentally measured mass of the  $X(3915)$ .

In parallel, detailed analyses of doubly heavy tetraquark states such as  $T_{cc}$  and  $T_{bb}$ , which contain open heavy flavors, have shown that their internal structures are typically dominated by color triplet components due to strong correlation of the light diquark, with distinct features arising from different admixtures of color triplet and color sextet configurations [25]. These results highlight the crucial role played by color-spin interactions in binding quarks together in tetraquark configurations. However, the  $X(3915)$  differs fundamentally from these states in that it possesses a hidden flavor  $c\bar{c}ss\bar{s}$  quark composition, for which diquark correlations are expected to be suppressed due to the masses of heavy quarks. Although its mass lies close to a relevant hadronic decay threshold, similar to the case of the  $T_{cc}$ , the absence of open heavy flavors and the presence of both charm and strange quarks may lead to qualitatively different color-spin dynamics and internal color configurations. As a consequence, the internal structure of the  $X(3915)$  cannot be directly inferred from the patterns observed in doubly heavy open flavor tetraquarks. A dedicated investigation of the color-spin structure specific to a  $c\bar{c}ss\bar{s}$  configuration associated with the  $X(3915)$ , together with an investigation of how different internal structures give rise to distinct experimentally accessible observables, is therefore essential.

\* [sungtae.cho@kangwon.ac.kr](mailto:sungtae.cho@kangwon.ac.kr)

† [aaron.park@yonsei.ac.kr](mailto:aaron.park@yonsei.ac.kr)

‡ [suhoung@yonsei.ac.kr](mailto:suhoung@yonsei.ac.kr)

§ [sungsiknoh@kangwon.ac.kr](mailto:sungsiknoh@kangwon.ac.kr)

In this work, we employ a quark model based on a full model Hamiltonian that includes a Yukawa type hyperfine potential, which has been shown to reproduce hadron masses accurately even when a single dominant spatial basis is adopted [26]. We calculate the mass of the  $X(3915)$  and precisely reproduce the experimentally measured value, thereby providing a more reliable foundation for investigating its internal structure.

Furthermore, we investigate the internal structure and production of the  $X(3915)$  in relativistic heavy ion collisions based on a coalescence model, by calculating the transverse momentum distributions and yields for various proposed states of the  $X(3915)$ , i.e., a charmonium, a tetraquark, and a hadronic molecular state. As it has been known that the yield of exotic hadrons strongly depends on their internal structures [20–22], we expect to be able to provide a detailed assessment of whether the  $X(3915)$  behaves more like a hadronic molecular or a compact multiquark state by analyzing the internal color-spin structure and studying production in relativistic heavy ion collisions through a coalescence model. Compared to previous studies, our approach explicitly connects the internal quark configuration to observable production characteristics, offering a unique perspective on the nature of the  $X(3915)$ .

Here, we assume that the  $X(3915)$  exists in a  $2p$  state when the  $X(3915)$  meson is produced as a charmonium state, though its internal structure is still unclear, and its existence as a  $2p$  state, the  $\chi_{c0}(2P)$  has been refuted because of inconsistencies in its decay modes and widths compared to theoretical evaluations [29, 30]. Concerning the production of the  $X(3915)$  in a tetraquark state, we regard the  $X(3915)$  as the  $c\bar{c}s\bar{s}$  state, while we consider the  $D_s\bar{D}_s$  for the  $X(3915)$  in a hadronic molecular state.

The paper is organized as follows. In Sec. II, we first briefly describe the simplified quark model. In Sec. III, we then analyze internal color-spin structure of the  $X(3915)$  based on the quark model calculations. In Sec. IV, we introduce the yield and transverse momentum distribution within the coalescence model to consider the production of  $X(3915)$  mesons by recombination in relativistic heavy ion collisions for three possible states of the  $X(3915)$ , i.e., a charmonium, a tetraquark, and a hadronic molecular state. Then, in Sec. V we calculate the yield and transverse momentum distribution of the  $X(3915)$ , and present the transverse momentum distribution ratio between the  $X(3915)$  and  $D_s$ . We also discuss the possibilities of identifying the internal structure of the  $X(3915)$  meson from its production in heavy ion collisions in Sec. V. The Sec. VI is devoted to conclusions.

## II. QUARK MODEL DESCRIPTION

To analyze the short range part of the interaction, we adopt a simplified quark model described in Ref. [23]. However, as shown in Refs. [25, 26], the Yukawa type hyperfine potential is more suitable for describing short

range interactions than the Gaussian type used in Ref. [23]. In particular, as presented in Ref. [26], the Yukawa type potential provides a good fit to hadron masses even when using only the most dominant single spatial basis in the calculations. We thus calculate the tetraquark state using only the most dominant single spatial basis and adopt the Yukawa type hyperfine potential from Ref. [26], instead of the Gaussian type used in Ref. [23]. With the Yukawa type hyperfine potential, the simplified quark model is described by the following Hamiltonian.

$$H = \sum_{i=1}^4 \left( m_i + \frac{\vec{p}_i^2}{2m_i} \right) - \frac{3}{4} \sum_{i < j}^4 \frac{\lambda_i^c}{2} \frac{\lambda_j^c}{2} (V_{ij}^C + V_{ij}^{CS} - D), \quad (1)$$

where the confinement and the Yukawa type hyperfine potentials are given as follows:

$$V_{ij}^C = -\frac{\kappa}{r_{ij}} + \sigma r_{ij}, \quad (2)$$

$$V_{ij}^{CS} = \frac{\mu_{ij}\mu'_{ij}}{m_i m_j c^4} \frac{\hbar c}{r_{ij}} e^{-\mu_{ij}r_{ij}/\hbar c} \vec{\sigma}_i \cdot \vec{\sigma}_j. \quad (3)$$

Here,  $m_i$  represents the quark mass,  $\lambda_i^c/2$  and  $\vec{\sigma}_i$  denote the SU(3) color and SU(2) spin operators, respectively, for the  $i$ th quark.  $r_{ij} \equiv |\vec{r}_i - \vec{r}_j|$  denotes the relative distance between the  $i$ th and  $j$ th quarks. Also,  $\mu_{ij}$  and  $\mu'_{ij}$  contain additional mass dependences as follows:

$$\mu_{ij} = \left( \alpha + \beta \frac{m_i m_j}{m_i + m_j} \right), \quad (4)$$

$$\mu'_{ij} = \left( \gamma + \delta \frac{m_i m_j}{m_i + m_j} \right). \quad (5)$$

We adopt the model fitting parameters determined from calculations using only the most dominant single spatial basis, as presented in Ref. [26], as follows:

$$\begin{aligned} \kappa &= 107.7 \text{ MeV fm}, \quad \sigma = 933.271 \text{ MeV/fm}, \quad D = 950 \text{ MeV}, \\ m_u &= 320 \text{ MeV}, \quad m_s = 612 \text{ MeV}, \quad m_c = 1893 \text{ MeV}, \\ \alpha &= 223.946 \text{ MeV}, \quad \beta = 0.227992, \\ \gamma &= 230.244 \text{ MeV}, \quad \delta = 0.315434, \end{aligned} \quad (6)$$

where we re-define a few parameters, compared to those of Ref. [26]. A few of the fitting results using the parameter set in Eq. (6) are shown in Table I. The full results for fitting to hadrons are found in Tables IV and V of Ref. [26].

The Jacobi coordinates describing the four-quark configuration, labelled by  $\bar{c}(1)\bar{s}(2)c(3)s(4)$ , can be set as follows:

(a) Coordinates Set 1

$$\begin{aligned} \vec{x}_1 &= \frac{1}{\sqrt{2}}(\vec{r}_1 - \vec{r}_4), & \vec{x}_2 &= \frac{1}{\sqrt{2}}(\vec{r}_2 - \vec{r}_3), \\ \vec{x}_3 &= \frac{1}{M_\mu} \left( \frac{m_1 \vec{r}_1 + m_4 \vec{r}_4}{m_1 + m_4} - \frac{m_2 \vec{r}_2 + m_3 \vec{r}_3}{m_2 + m_3} \right), \end{aligned} \quad (7)$$

TABLE I. This table shows the fitting results for a few of the hadron masses that are taken directly from Ref. [26] and obtained (Column 3) using the most dominant single spatial basis and the parameter set given in Eq. (6). Column 4 shows the variational parameters  $a_1$  and  $a_2$ . The results for all the other mesons and baryons are referred to Tables IV and V of Ref. [26].

Particle	Experimental Value (MeV)	Mass (MeV)	Variational Parameters (fm $^{-2}$ )	Error (%)
$D$	1864.8	1860.4	$a_1 = 4.4$	0.24
$D^*$	2007.0	2005.2	$a_1 = 3.5$	0.08
$\eta_c$	2983.6	2995.4	$a_1 = 14.3$	0.39
$J/\Psi$	3096.9	3117.5	$a_1 = 11.0$	0.67
$D_s$	1968.3	1961.0	$a_1 = 7.0$	0.37
$D_s^*$	2112.1	2097.6	$a_1 = 5.4$	0.69
$\Lambda_c$	2286.5	2265.4	$a_1 = 2.7, a_2 = 3.5$	0.92
$\Xi_{cc}$	3621.4	3609.6	$a_1 = 7.3, a_2 = 3.0$	0.33
$\Sigma_c$	2452.9	2444.6	$a_1 = 2.0, a_2 = 3.5$	0.37
$\Sigma_c^*$	2517.5	2528.2	$a_1 = 1.8, a_2 = 3.1$	0.39
$\Xi_c$	2467.8	2459.5	$a_1 = 3.1, a_2 = 4.4$	0.44
$\Xi_c^*$	2645.9	2639.9	$a_1 = 2.3, a_2 = 4.0$	0.24

(b) Coordinates Set 2

$$\vec{y}_1 = \frac{1}{\sqrt{2}}(\vec{r}_1 - \vec{r}_3), \quad \vec{y}_2 = \frac{1}{\sqrt{2}}(\vec{r}_4 - \vec{r}_2),$$

$$\vec{y}_3 = \frac{1}{M_\mu} \left( \frac{m_1 \vec{r}_1 + m_3 \vec{r}_3}{m_1 + m_3} - \frac{m_2 \vec{r}_2 + m_4 \vec{r}_4}{m_2 + m_4} \right), \quad (8)$$

(c) Coordinates Set 3

$$\vec{z}_1 = \frac{1}{\sqrt{2}}(\vec{r}_1 - \vec{r}_2), \quad \vec{z}_2 = \frac{1}{\sqrt{2}}(\vec{r}_3 - \vec{r}_4),$$

$$\vec{z}_3 = \frac{1}{M_\mu} \left( \frac{m_1 \vec{r}_1 + m_2 \vec{r}_2}{m_1 + m_2} - \frac{m_3 \vec{r}_3 + m_4 \vec{r}_4}{m_3 + m_4} \right), \quad (9)$$

where

$$M_\mu = \left[ \frac{m_1^2 + m_4^2}{(m_1 + m_4)^2} + \frac{m_2^2 + m_3^2}{(m_2 + m_3)^2} \right]^{1/2},$$

and

$$m_1 = m_3 = m_c, \quad m_2 = m_4 = m_s \quad \text{for } c\bar{c}ss\bar{s}.$$

We choose coordinates set 1 as our reference, as it is suitable for studying open flavor decay mode  $D_s\bar{D}_s$  of the  $X(3915)$ . Using the transformations between the different sets of Jacobi coordinates introduced above, we calculate the relevant matrix elements involving two quarks. We construct the spatial wave function in a simple Gaussian form, as follows:

$$\psi^{Spatial}(\vec{x}_1, \vec{x}_2, \vec{x}_3) = \left( \frac{2}{\pi} \right)^{\frac{9}{4}} a_1^{\frac{3}{4}} a_1^{\frac{3}{4}} a_3^{\frac{3}{4}} \exp \left[ -a_1 \vec{x}_1^2 - a_1 \vec{x}_2^2 - a_3 \vec{x}_3^2 \right], \quad (10)$$

where the variational parameter is set as  $a_2 = a_1$  to ensure that the spatial wave function is symmetric under the permutation (13)(24).

The color-spin(CS) wave function for the  $X(3915)$ , which has quantum numbers  $I^G(J^{PC}) = 0^+(0^{++})$ , is composed of four CS basis states:  $|CS'_1\rangle = |(\bar{c}c)_0^1(\bar{s}s)_0^1\rangle, |CS'_2\rangle = |(\bar{c}c)_0^8(\bar{s}s)_0^8\rangle, |CS'_3\rangle = |(\bar{c}c)_1^1(\bar{s}s)_1^1\rangle, |CS'_4\rangle = |(\bar{c}c)_1^8(\bar{s}s)_1^8\rangle$ , where  $c$  and  $s$  denote charm and strange quarks, respectively. The superscripts(subscripts) indicate the color(spin) states of each quark-antiquark pair. These CS bases can be represented through a different quark-antiquark basis,  $(\bar{c}s) \otimes (\bar{s}c)$ , as follows:

$$|CS'_1\rangle = -\frac{1}{2\sqrt{3}}|CS_1\rangle + \frac{1}{6}|CS_2\rangle - \sqrt{\frac{2}{3}}|CS_3\rangle + \frac{\sqrt{2}}{3}|CS_4\rangle,$$

$$|CS'_2\rangle = -\sqrt{\frac{2}{3}}|CS_1\rangle + \frac{\sqrt{2}}{3}|CS_2\rangle + \frac{1}{2\sqrt{3}}|CS_3\rangle - \frac{1}{6}|CS_4\rangle,$$

$$|CS'_3\rangle = -\frac{1}{6}|CS_1\rangle - \frac{1}{2\sqrt{3}}|CS_2\rangle - \frac{\sqrt{2}}{3}|CS_3\rangle - \sqrt{\frac{2}{3}}|CS_4\rangle,$$

$$|CS'_4\rangle = -\frac{\sqrt{2}}{3}|CS_1\rangle - \sqrt{\frac{2}{3}}|CS_2\rangle + \frac{1}{6}|CS_3\rangle + \frac{1}{2\sqrt{3}}|CS_4\rangle, \quad (11)$$

where  $|CS_1\rangle = |(\bar{c}s)_1^1(\bar{s}c)_1^1\rangle, |CS_2\rangle = |(\bar{c}s)_0^1(\bar{s}c)_0^1\rangle, |CS_3\rangle = |(\bar{c}s)_1^8(\bar{s}c)_1^8\rangle, |CS_4\rangle = |(\bar{c}s)_0^8(\bar{s}c)_0^8\rangle$ . However, for the analysis of the open flavor decay channel  $D_s\bar{D}_s$ , it is more appropriate to represent the four CS states in the  $(\bar{c}s) \otimes (\bar{s}c)$  basis, which better reflects the structure of the final state of the  $D_s\bar{D}_s$  mesons. This can be obtained through an orthogonal transformation from the original basis set of Eq. (11). The transformed CS basis states are given as follows:

$$|CS_1\rangle = -\frac{1}{2\sqrt{3}}|CS'_1\rangle - \sqrt{\frac{2}{3}}|CS'_2\rangle - \frac{1}{6}|CS'_3\rangle - \frac{\sqrt{2}}{3}|CS'_4\rangle,$$

$$|CS_2\rangle = \frac{1}{6}|CS'_1\rangle + \frac{\sqrt{2}}{3}|CS'_2\rangle - \frac{1}{2\sqrt{3}}|CS'_3\rangle - \sqrt{\frac{2}{3}}|CS'_4\rangle,$$

$$|CS_3\rangle = -\sqrt{\frac{2}{3}}|CS'_1\rangle + \frac{1}{2\sqrt{3}}|CS'_2\rangle - \frac{\sqrt{2}}{3}|CS'_3\rangle + \frac{1}{6}|CS'_4\rangle,$$

$$|CS_4\rangle = \frac{\sqrt{2}}{3}|CS'_1\rangle - \frac{1}{6}|CS'_2\rangle - \sqrt{\frac{2}{3}}|CS'_3\rangle + \frac{1}{2\sqrt{3}}|CS'_4\rangle. \quad (12)$$

### III. SHORT RANGE INTERACTION

As shown in Table II, the quark model calculation for the Hamiltonian in Eq. (1) gives the ground state mass of 3922.1 MeV, which exactly reproduces the measured mass of the  $X(3915)$ . The parameters  $a_1$  and  $a_3$  are determined through a variational method applied to the ground state. As the variational parameter  $a_3$  goes to 0, the ground state mass of the  $X(3915)$  approaches its

threshold value. Furthermore, the parameter  $a_1$  is the same as that for the  $D_s$  meson given in Table I. This implies that the tetraquark wave function reduces to those of its threshold.

TABLE II. Masses of the  $X(3915)$  and the corresponding thresholds, calculated using the full model Hamiltonian given in Eq. (1). The threshold masses are obtained from the masses of the threshold mesons presented in Table I.

Configuration	$J^{PC}$	Threshold(MeV)	Measured mass(MeV)	Mass(MeV)	Variational parameters (fm $^{-2}$ )
$c\bar{c}s\bar{s}$	$0^{++}$	$D_s\bar{D}_s(3922.0)$	3922.1	3922.1	$a_1 = 7.0, a_3 = 0.001$

To investigate the short distance part of interaction, we adopt the color-spin factor  $K$ , defined in Ref. [19], as follows:

$$K = - \sum_{i < j}^n \frac{1}{m_i m_j} \lambda_i^c \lambda_j^c \vec{\sigma}_i \cdot \vec{\sigma}_j, \quad (13)$$

$$K_{X(3915)} =$$

$$\begin{pmatrix} \frac{16}{3} \left( \frac{1}{m_{\bar{c}} m_s} + \frac{1}{m_{\bar{s}} m_c} \right) & 0 & \frac{8\sqrt{2}(m_{\bar{c}} - m_s)(m_{\bar{s}} - m_c)}{3m_{\bar{c}} m_{\bar{s}} m_c m_s} & \frac{4\sqrt{2}(m_{\bar{c}} + m_s)(m_{\bar{s}} + m_c)}{\sqrt{3}m_{\bar{c}} m_{\bar{s}} m_c m_s} & \frac{4\sqrt{2}(m_{\bar{c}} + m_s)(m_{\bar{s}} + m_c)}{\sqrt{3}m_{\bar{c}} m_{\bar{s}} m_c m_s} \\ 0 & -\frac{16}{m_{\bar{c}} m_s} - \frac{16}{m_{\bar{s}} m_c} & \frac{4\sqrt{2}(m_{\bar{c}} + m_s)(m_{\bar{s}} + m_c)}{\sqrt{3}m_{\bar{c}} m_{\bar{s}} m_c m_s} & 0 & 0 \\ \frac{8\sqrt{2}(m_{\bar{c}} - m_s)(m_{\bar{s}} - m_c)}{3m_{\bar{c}} m_{\bar{s}} m_c m_s} & \frac{4\sqrt{2}(m_{\bar{c}} + m_s)(m_{\bar{s}} + m_c)}{\sqrt{3}m_{\bar{c}} m_{\bar{s}} m_c m_s} & \frac{-8m_c m_s - (28m_c + 2m_s + 8m_{\bar{s}})m_{\bar{c}} - (2m_c + 28m_s)m_{\bar{s}}}{3m_{\bar{c}} m_{\bar{s}} m_c m_s} & \frac{-4m_c m_s + 14m_{\bar{c}} m_c + 14m_{\bar{s}} m_s - 4m_{\bar{c}} m_{\bar{s}}}{\sqrt{3}m_{\bar{c}} m_{\bar{s}} m_c m_s} & \frac{2}{m_{\bar{c}} m_s} + \frac{2}{m_{\bar{s}} m_c} \\ \frac{4\sqrt{2}(m_{\bar{c}} + m_s)(m_{\bar{s}} + m_c)}{\sqrt{3}m_{\bar{c}} m_{\bar{s}} m_c m_s} & 0 & \frac{-4m_c m_s + 14m_{\bar{c}} m_c + 14m_{\bar{s}} m_s - 4m_{\bar{c}} m_{\bar{s}}}{\sqrt{3}m_{\bar{c}} m_{\bar{s}} m_c m_s} & \frac{2}{m_{\bar{c}} m_s} + \frac{2}{m_{\bar{s}} m_c} & \end{pmatrix}, \quad (14)$$

where the matrix is expressed in the CS bases given in Eq. (12). The quark masses are presented separately for antiquarks and quarks. By subtracting the threshold term  $-\frac{16}{m_{\bar{c}} m_s} - \frac{16}{m_{\bar{s}} m_c}$  from the diagonal elements, one can obtain the effective attraction coming from the color-spin interaction factor,  $K_{X(3915)} - K_{D_s} - K_{\bar{D}_s}$ .

For a tetraquark configuration, there are four CS bases for total spin 0 and six CS bases for total spin 1[23]. For the  $X(3915)$  with total spin 0, all four CS bases satisfy the charge conjugation symmetry, whereas in tetraquarks with similar structures but total spin 1, such as the  $X(3872)$ , this is not the case. In fact, as noted in Ref. [19], only two of the six CS bases satisfy the quantum number constraints of the  $X(3872)$ , corresponding to the color singlet and color octet bases with the same spin structures. This leads to mixing terms between color singlet and color octet bases for the  $X(3915)$ , as reflected in the non-zero off-diagonal elements of Eq. (14).

When analyzing the diagonal elements of Eq. (14), one finds that the expectation value corresponding to the  $|CS_3\rangle$  state has a more intricate structure compared to those of the  $|CS_1\rangle$ ,  $|CS_2\rangle$ , and  $|CS_4\rangle$  basis states. This difference arises because, within color SU(3) and spin SU(2), the color-color and spin-spin expectation values

where  $\lambda_i^c$  and  $\sigma_i$  are the color and spin operators, respectively, and  $m_i$  the mass of the  $i$ th quark among the  $n$  quarks. The  $K$  factor for the  $X(3915)$  in the CS bases given in Eq. (12) is as follows:

vanish for quark pairs directly coupled in singlet-singlet configurations of either the color or spin state. Consequently, for the  $|CS_1\rangle$ ,  $|CS_2\rangle$ , and  $|CS_4\rangle$  bases, only the  $(\bar{c}s)$  and  $(\bar{s}c)$  pairs contribute. In contrast, the  $|CS_3\rangle$  basis corresponds to a color octet-octet and spin triplet-triplet configuration, for which the expectation values do not vanish, leading to nonzero contributions from all possible quark pairs.

On the other hand, from the diagonal elements of Eq. (14), one might naively expect that the dominant contribution to the  $X(3915)$  arises from the CS basis  $|CS_3\rangle$ , corresponding to the color octet and spin 1 states for both the  $(\bar{c}s)$  and  $(\bar{s}c)$  pairs. This is based on the fact that, as shown from the (3,3) component of Eq. (14), there exists an attractive contribution coming from the interaction of the  $s\bar{s}$  pair, which is not suppressed by the relatively large charm quark mass  $m_c$ . This attraction comes from the  $|CS'_1\rangle$ , which corresponds to the color singlet and spin 0 for the  $s\bar{s}$  pair contained in the  $|CS_3\rangle$  state, as shown in Eq. (12).

However, once the full hyperfine interaction is evaluated by incorporating the spatial wave functions, the actual dominant attractive contribution is found to come from the CS basis  $|CS_2\rangle$ , which corresponds to the color

singlet and spin 0 states for both the  $(\bar{c}s)$  and  $(\bar{s}c)$  pairs, i.e., the  $D_s\bar{D}_s$  threshold configuration. This difference arises because the actual contribution of the hyperfine potential depends not only on the color-spin factors but also on the spatial factor, which depends on the sizes of the individual quark pairs and, therefore, varies from pair to pair. In particular, when the  $D_s\bar{D}_s$  threshold mesons are largely separated, the distance between the  $s$  and  $\bar{s}$  quarks becomes large, leading to a suppression of their hyperfine interaction despite the favorable color-spin factor. By combining the spatial factors associated with the variational parameters determined for the ground state of the  $X(3915)$  and using the model parameters given in Eq. (6), the hyperfine potential matrix in Eq. (1) is evaluated in MeV unit as follows:

$$\langle H^{Hyp} \rangle = \begin{pmatrix} 74.99 & 0 & -0.41 & 0.36 \\ 0 & -224.95 & 0.36 & 0 \\ -0.41 & 0.36 & -10.39 & 0.88 \\ 0.36 & 0 & 0.88 & 28.12 \end{pmatrix}, \quad (15)$$

where  $H^{Hyp} = -\frac{3}{4} \sum_{i < j}^4 \frac{\lambda_i^c}{2} \frac{\lambda_j^c}{2} V_{ij}^{CS}$ . As shown in Eq. (15), the contribution from the  $|CS_2\rangle$  is clearly dominant. This is further supported by the probability amplitudes listed in Table III, which shows the contributions of each CS basis to the ground state wave function of the  $X(3915)$ , obtained through the variational method. From Table III, it is also evident that the ground state wave function of the  $X(3915)$  expanded by the CS basis set of Eq. (12) corresponds to a well-separated  $D_s\bar{D}_s$  configuration.

TABLE III. Probability amplitudes for each color-spin state in the ground state wave function of the  $X(3915)$ . The sets of color-spin bases in the table are defined in Eqs. (11) and (12).

CS basis set	Amplitudes
$\{ CS_1\rangle,  CS_2\rangle,  CS_3\rangle,  CS_4\rangle\}$	$\{0.0, 1.0, 0.0, 0.0\}$
$\{ CS'_1\rangle,  CS'_2\rangle,  CS'_3\rangle,  CS'_4\rangle\}$	$\{0.03, 0.22, 0.08, 0.67\}$

As shown in Table III, the probability amplitudes obtained in a different basis set provide additional insight on the internal structure of the  $X(3915)$  that the relative contributions of each quark pair in the tetraquark configuration of the  $X(3915)$ . In particular, from Eq. (12), the transformation of the  $|CS_2\rangle$  shows that the probability amplitudes obtained in the  $(\bar{c}c) \otimes (\bar{s}s)$  basis are equivalent to the square of coefficients of each  $(\bar{c}c) \otimes (\bar{s}s)$  basis. In this transformation, the CS basis  $|CS'_4\rangle$  has the largest probability amplitude. This basis, in which both the  $(\bar{c}c)$  and  $(\bar{s}s)$  pairs are in color octet and spin 1 configurations, is structurally analogous to the dominant contributing basis for the  $X(3872)$ , which has a similar configuration but total spin 1.

Furthermore, considering a well-separated  $D_s\bar{D}_s$  configuration, one can ignore the  $1/(m_{\bar{c}}m_c)$ ,  $1/(m_{\bar{s}}m_s)$ ,

$1/(m_{\bar{c}}m_{\bar{s}})$ , and  $1/(m_cm_s)$  terms in Eq. (14), corresponding to  $(\bar{c}c)$ ,  $(\bar{s}s)$ ,  $(\bar{c}s)$ , and  $(cs)$  pairs, respectively. In this limit, Eq. (14) reduces to the following diagonal matrix.

$$K_{X(3915)} = \begin{pmatrix} \frac{32}{3m_cm_s} & 0 & 0 & 0 \\ 0 & -\frac{32}{m_cm_s} & 0 & 0 \\ 0 & 0 & -\frac{4}{3m_cm_s} & 0 \\ 0 & 0 & 0 & \frac{4}{m_cm_s} \end{pmatrix}, \quad (16)$$

where we take only the contributions corresponding to the threshold mesons and  $m_{\bar{q}} = m_q$ . This further indicates that the ground state we calculate corresponds to a well-separated  $D_s\bar{D}_s$  configuration. The off-diagonal elements in Eq. (15) vanish as the variational parameter  $a_3 \rightarrow 0$ , corresponding to this well-separated  $D_s\bar{D}_s$  configuration, and the ratios of the diagonal elements reduce to those in Eq. (16). This suggests that the  $X(3915)$  is unlikely to correspond to a compact configuration and is instead more consistent with a molecular structure, originating from the long-range interactions that extend beyond the scope of this model. Nevertheless, although we find that the ground state favors a separated  $D_s\bar{D}_s$  configuration, the model has an intrinsic uncertainty on the order of a few MeV, as shown in Table I. Consequently, a compact tetraquark structure cannot be conclusively ruled out.

In the following section, we study the possibility of experimentally discriminating among different candidate structures of the  $X(3915)$  by analyzing additional physical observables associated with its production in heavy ion collisions within the framework of the coalescence model.

#### IV. PRODUCTION OF THE $X(3915)$ MESON IN HEAVY ION COLLISIONS

We consider here  $X(3915)$  mesons produced from various constituents by coalescence in relativistic heavy ion collisions. Adopting the coalescence picture for the formation of the meson [31, 32], we evaluate the yield and transverse momentum distribution of the  $X(3915)$  in a  $\bar{c}c$  charmonium, a  $\bar{c}c\bar{s}s$  tetraquark, or a  $D_s\bar{D}_s$  hadronic molecular state, denoted by  $X_{c\bar{c}}$ ,  $X_{c\bar{c}\bar{s}s}$ , and  $X_{D_s\bar{D}_s}$ , respectively.

##### A. The $X(3915)$ meson in a two-quark state

As mentioned before, we consider the  $X(3915)$  as a  $\bar{c}c$  state with an internal relative momentum, i.e., a  $2p$ -wave state. When the  $X(3915)$  meson is produced from one charm and one anti-charm quarks in the quark-gluon plasma by charm quark recombination, the production process of the  $X(3915)$  meson is similar to those of the  $J/\psi$ ,  $\chi_{c1}(1P)$ , and  $\psi(2S)$  mesons since the  $X(3915)$  has the same quark contents as the above charmonium states except for its different  $2p$  internal structure. Then,

the transverse momentum distribution of the  $X(3915)$  is given by [33, 34],

$$\frac{d^2N_{X_{c\bar{c}}}}{d^2\vec{p}_T} = \frac{g_X}{V} \int d^3\vec{r} d^2\vec{p}_{\bar{c}T} d^2\vec{p}_{cT} W_{2p}(\vec{r}, \vec{k}) \times \frac{d^2N_{\bar{c}}}{d^2\vec{p}_{\bar{c}T}} \frac{d^2N_c}{d^2\vec{p}_{cT}} \delta^{(2)}(\vec{p}_T - \vec{p}_{\bar{c}T} - \vec{p}_{cT}), \quad (17)$$

in the non-relativistic limit. In Eq. (17) the assumption on the boost-invariant longitudinal momentum distributions for constituents satisfying  $\eta = y$  between spatial,  $\eta$  and momentum  $y$  rapidities, or the Bjorken correlation has been made. The  $g_X$  is the degeneracy factor for possible chances of producing the  $X(3915)$  meson from its constituents, e.g.,  $g_X = 1/(2 \cdot 3)^2$ .

The  $\vec{r}$  and  $\vec{k}$  in Eq. (17) are a relative distance and a relative transverse momentum between charm and anti-charm quarks, respectively, in the rest frame of the  $X(3915)$ . We take here the following configurations and relative transverse momenta for charm and anti-charm quarks,

$$\vec{R} = \frac{m_{\bar{c}}\vec{r}_{\bar{c}} + m_c\vec{r}_c}{m_{\bar{c}} + m_c}, \quad \vec{r} = \vec{r}_{\bar{c}} - \vec{r}_c, \\ \vec{K} = \vec{p}'_{\bar{c}T} + \vec{p}'_{cT}, \quad \vec{k} = \frac{m_c\vec{p}'_{\bar{c}T} - m_{\bar{c}}\vec{p}'_{cT}}{m_{\bar{c}} + m_c}. \quad (18)$$

The relative transverse momentum  $\vec{k}$  connects transverse momenta of constituent quarks in two different frames, i.e., between  $\vec{p}_{\bar{c}T}$  and  $\vec{p}_{cT}$  in the fireball frame and  $\vec{p}'_{\bar{c}T}$  and  $\vec{p}'_{cT}$  in the  $X(3915)$  rest frame by Lorentz transformation [35, 36]. The transverse momentum distribution difference between the  $X(3915)$  and other charmonium states in two-quark states in the coalescence model originates from this Lorentz transformation, as the mass difference between the  $X(3915)$  and other charmonium states causes different Lorentz transformation from the fireball frame to the rest frame of the meson.

In regard to the  $2p$ -wave Wigner function, we construct it based on harmonic oscillator wave functions in three dimensions,

$$\psi_{11m}(\vec{r}) = \frac{1}{(\pi\sigma^2)^{1/4}} \frac{4}{\sqrt{15}} \frac{r}{\sigma^2} \left( \frac{5}{2} - \frac{r^2}{\sigma^2} \right) e^{-\frac{r^2}{2\sigma^2}} Y_{1m}(\theta, \phi), \quad (19)$$

with  $\sigma^2 = 1/(\mu\omega)$  relating the oscillator frequency of the harmonic oscillator wave function,  $\omega$  and the reduced mass,  $\mu = m_{\bar{c}}m_c/(m_{\bar{c}} + m_c)$ . In Eq. (19), the subscript  $11m$  in the wave function  $\psi_{11m}(\vec{r})$  represents the quantum number  $klm$  in the three dimensional harmonic oscillator, i.e., the energy  $E_n = (n+3/2)\hbar\omega$  with  $n = 2k+l$ , and  $Y_{lm}(\theta, \phi)$  is the spherical harmonics.

Using the  $m$ -averaged density for  $2p$  states, similar to that for  $1d$  states [21],

$$\rho(\vec{r}, \vec{r}') = \frac{1}{3} \sum_m \psi_{11m}(\vec{r}) \psi_{11m}^*(\vec{r}') \quad (20)$$

we build the Wigner function,

$$W(\vec{r}, \vec{k}) = \int d^3\vec{q} \rho\left(\vec{r} + \frac{\vec{q}}{2}, \vec{r} - \frac{\vec{q}}{2}\right) e^{i\vec{k}\cdot\vec{q}} \quad (21)$$

resulting in,

$$W_{2p}(\vec{r}, \vec{k}) = \frac{15}{32} e^{-\frac{r^2}{\sigma^2} - k^2\sigma^2} \left( \frac{r^6}{\sigma^6} - \frac{11}{2} \frac{r^4}{\sigma^4} + \frac{15}{2} \frac{r^2}{\sigma^2} + \frac{15}{2} k^2\sigma^2 \right. \\ \left. - \frac{11}{2} k^4\sigma^4 + k^6\sigma^6 + r^2 k^2 \left( 3 - \frac{r^2}{\sigma^2} - k^2\sigma^2 \right) \right. \\ \left. + 2(\vec{r} \cdot \vec{k}) \left( -7 + 2 \frac{r^2}{\sigma^2} + 2k^2\sigma^2 \right) - \frac{15}{4} \right). \quad (22)$$

The  $2p$ -Wigner function in Eq. (22) is consistent with the previous result [37], and satisfies,

$$\int d^3\vec{r} W_{2p}(\vec{r}, \vec{k}) = \frac{1}{3} \sum_m \tilde{\psi}_{11m}(\vec{k}) \tilde{\psi}_{11m}^*(\vec{k}) \quad (23)$$

with the three dimensional harmonic oscillator wave function in momentum space,  $\tilde{\psi}_{11m}(\vec{k})$ .

Adopting the above  $2p$ -Wigner function in Eq. (22) to the transverse momentum distribution of the  $X(3915)$  in a  $2p$  charmonium state in Eq. (17) yields,

$$\frac{d^2N_{X_{c\bar{c}}}}{d^2\vec{p}_T} = \frac{g_X}{V} (2\sqrt{\pi}\sigma)^3 \int d^2\vec{p}_{\bar{c}T} d^2\vec{p}_{cT} \frac{d^2N_{\bar{c}}}{d^2\vec{p}_{\bar{c}T}} \frac{d^2N_c}{d^2\vec{p}_{cT}} \\ \times \frac{4}{15} \sigma^2 k^2 e^{-\sigma^2 k^2} \left( k^2\sigma^2 - \frac{5}{2} \right)^2 \delta^{(2)}(\vec{p}_T - \vec{p}_{\bar{c}T} - \vec{p}_{cT}). \quad (24)$$

## B. The $X(3915)$ meson in a four-quark state

Next, we calculate the transverse momentum distribution of the  $X(3915)$  meson when it exists in a four-quark state: the  $X(3915)$  meson is produced from one strange, one anti-strange, one charm and one anti-charm quarks in the quark-gluon plasma by coalescence. All quarks inside the  $X(3915)$  in a four-quark state reside in a  $s$ -wave, consistent with its spin and parity,  $J^P = 0^+$ .

The transverse momentum distribution of the  $X(3915)$  meson in a four-quark state is taken from that of the  $X(3872)$  meson in a four-quark state [38], replacing two light quarks with two strange quarks,

$$\frac{d^2N_{X_{c\bar{c}ss\bar{s}}}}{d^2\vec{p}_T} = \frac{g_X}{V^3} (2\sqrt{\pi})^9 (\sigma_1\sigma_2\sigma_3)^3 \\ \times \int d^2\vec{p}_{sT} d^2\vec{p}_{\bar{s}T} d^2\vec{p}_{cT} d^2\vec{p}_{\bar{c}T} \\ \times \frac{d^2N_s}{d^2\vec{p}_{sT}} \frac{d^2N_{\bar{s}}}{d^2\vec{p}_{\bar{s}T}} \frac{d^2N_c}{d^2\vec{p}_{cT}} \frac{d^2N_{\bar{c}}}{d^2\vec{p}_{\bar{c}T}} \\ \times \delta^{(2)}(\vec{p}_T - \vec{p}_{sT} - \vec{p}_{\bar{s}T} - \vec{p}_{cT} - \vec{p}_{\bar{c}T}) \\ \times \exp\left(-\sigma_1^2 k_1^2 - \sigma_2^2 k_2^2 - \sigma_3^2 k_3^2\right), \quad (25)$$

with relative coordinates,

$$\begin{aligned}\vec{R}_{4q} &= \frac{m_s \vec{r}_s + m_{\bar{s}} \vec{r}_{\bar{s}} + m_c \vec{r}_c + m_{\bar{c}} \vec{r}_{\bar{c}}}{m_s + m_{\bar{s}} + m_c + m_{\bar{c}}}, \\ \vec{r}_1 &= \vec{r}_s - \vec{r}_{\bar{s}}, \\ \vec{r}_2 &= \frac{m_s \vec{r}_s + m_{\bar{s}} \vec{r}_{\bar{s}}}{m_s + m_{\bar{s}}} - \vec{r}_c, \\ \vec{r}_3 &= \frac{m_s \vec{r}_s + m_{\bar{s}} \vec{r}_{\bar{s}} + m_c \vec{r}_c}{m_s + m_{\bar{s}} + m_c} - \vec{r}_{\bar{c}},\end{aligned}\quad (26)$$

and corresponding relative transverse momenta,

$$\begin{aligned}\vec{k}_{4q} &= \vec{p}'_{sT} + \vec{p}'_{\bar{s}T} + \vec{p}'_{cT} + \vec{p}'_{\bar{c}T}, \\ \vec{k}_1 &= \frac{m_{\bar{s}} \vec{p}'_{sT} - m_s \vec{p}'_{\bar{s}T}}{m_s + m_{\bar{s}}}, \\ \vec{k}_2 &= \frac{m_c (\vec{p}'_{sT} + \vec{p}'_{\bar{s}T}) - (m_s + m_{\bar{s}}) \vec{p}'_{cT}}{m_s + m_{\bar{s}} + m_c}, \\ \vec{k}_3 &= \frac{m_{\bar{c}} (\vec{p}'_{sT} + \vec{p}'_{\bar{s}T} + \vec{p}'_{cT}) - (m_s + m_{\bar{s}} + m_c) \vec{p}'_{\bar{c}T}}{m_s + m_{\bar{s}} + m_c + m_{\bar{c}}}.\end{aligned}\quad (27)$$

In Eq. (27), the transverse momenta of quarks,  $\vec{p}'_{qT}$  ( $q = s, \bar{s}, c, \bar{c}$ ) are the transverse momenta in the rest frame of the  $X(3915)$  meson, obtained from those in the fireball frame,  $\vec{p}_q$  by Lorentz transformation as mentioned in the previous section. The  $\sigma_1$ ,  $\sigma_2$  and  $\sigma_3$  in Eq. (25) are related to the oscillator frequency of the harmonic oscillator wave function  $\omega$  in the  $s$ -wave Wigner function,

$$\begin{aligned}W_{c\bar{c}ss}(\vec{r}_1, \vec{r}_2, \vec{r}_3, \vec{k}_1, \vec{k}_2, \vec{k}_3) &= 8^3 \exp\left(-\frac{r_1^2}{\sigma_1^2} - \sigma_1^2 k_1^2\right) \exp\left(-\frac{r_2^2}{\sigma_2^2} - \sigma_2^2 k_2^2\right) \\ &\times \exp\left(-\frac{r_3^2}{\sigma_3^2} - \sigma_3^2 k_3^2\right),\end{aligned}\quad (28)$$

with reduced masses,

$$\begin{aligned}\mu_1 &= \frac{m_s m_{\bar{s}}}{m_s + m_{\bar{s}}}, \quad \mu_2 = \frac{(m_s + m_{\bar{s}}) m_c}{m_s + m_{\bar{s}} + m_c}, \\ \mu_3 &= \frac{(m_s + m_{\bar{s}} + m_c) m_{\bar{c}}}{m_s + m_{\bar{s}} + m_c + m_{\bar{c}}},\end{aligned}\quad (29)$$

corresponding to  $\sigma_1^2 = 1/(\omega \mu_1)$ ,  $\sigma_2^2 = 1/(\omega \mu_2)$ , and  $\sigma_3^2 = 1/(\omega \mu_3)$ , respectively.

In taking the relative configurations between four quarks, one may choose other coordinates and momenta rather than Eqs. (26) and (27). However, it has been shown that the yield and transverse momentum distribution are not dependent on different choices for relative coordinates and momenta between quarks inside the hadron when all quarks are in the ground state, suitable for the  $s$ -wave Gaussian Wigner function, Eq. (28) with one oscillator frequency  $\omega$  [38]. We take the oscillator frequency, 0.103 GeV [39] in Eqs. (17) and (25).

### C. The $X(3915)$ meson in a hadronic molecular state

When the  $X(3915)$  meson is in a hadronic molecular state made up of  $D_s$  and  $\bar{D}_s$  mesons, the yield and transverse momentum distribution of it can be obtained by replacing charm and anti-charm quarks with  $D_s$  and  $\bar{D}_s$  mesons, respectively in Eq. (17). Thus, the transverse momentum distribution of the  $X_{D_s \bar{D}_s}$  is given by,

$$\begin{aligned}\frac{d^2 N_{X_{D_s \bar{D}_s}}}{d^2 \vec{p}_T} &= \frac{g_X}{V} (2\sqrt{\pi} \sigma_h)^3 \int d^2 \vec{p}_{D_s T} d^2 \vec{p}_{\bar{D}_s T} e^{-\sigma_h^2 k^2} \\ &\times \frac{d^2 N_{D_s}}{d^2 \vec{p}_{D_s T}} \frac{d^2 N_{\bar{D}_s}}{d^2 \vec{p}_{\bar{D}_s T}} \delta^{(2)}(\vec{p}_T - \vec{p}_{\bar{D}_s T} - \vec{p}_{D_s T}),\end{aligned}\quad (30)$$

with relative coordinates and transverse momenta between  $D_s$  and  $\bar{D}_s$  mesons,

$$\begin{aligned}\vec{R}_h &= \frac{m_{\bar{D}_s} \vec{r}_{\bar{D}_s} + m_{D_s} \vec{r}_{D_s}}{m_{\bar{D}_s} + m_{D_s}}, \quad \vec{r}_h = \vec{r}_{\bar{D}_s} - \vec{r}_{D_s}, \\ \vec{K}_h &= \vec{p}'_{\bar{D}_s T} + \vec{p}'_{D_s T}, \quad \vec{k}_h = \frac{m_{D_s} \vec{p}'_{\bar{D}_s T} - m_{\bar{D}_s} \vec{p}'_{D_s T}}{m_{\bar{D}_s} + m_{D_s}},\end{aligned}\quad (31)$$

again with the relative transverse momentum  $\vec{k}_h$  connecting transverse momenta of  $D_s$  and  $\bar{D}_s$  mesons between  $\vec{p}_{\bar{D}_s T}$  and  $\vec{p}_{D_s T}$  in the fireball frame and  $\vec{p}'_{\bar{D}_s T}$  and  $\vec{p}'_{D_s T}$  in the rest frame of the  $X(3915)$  in a hadronic molecular state by Lorentz transformation.

In Eq. (31), the  $s$ -wave Wigner function,

$$W_s(\vec{r}, \vec{k}) = 8e^{-\frac{r^2}{\sigma_h^2} - k^2 \sigma_h^2}\quad (32)$$

has already been adopted with both the  $\sigma_h$ , representing the oscillator frequency of the harmonic wave function in the Wigner function, and the reduced mass,  $\mu_h = m_{D_s} m_{\bar{D}_s} / (m_{D_s} + m_{\bar{D}_s})$ . We take the oscillator frequency, 0.0876 GeV obtained from the relation between the binding energy and the oscillator frequency [21],  $\omega = 6E_B$ , with the binding energy of the  $X(3915)$ ,  $E_B = M_{D_s} + M_{\bar{D}_s} - M_{X(3915)} = 1968.35 \times 2 - 3922.1 = 14.6$  (MeV).

### V. YIELDS AND TRANSVERSE MOMENTUM DISTRIBUTIONS OF THE $X(3915)$

We evaluate the transverse momentum distributions of  $X(3915)$  mesons using Eqs. (24), (25) and (30) when they are produced as either charmonium states, four-quark states, or hadronic molecular states from their constituents by recombination in heavy ion collisions at

$\sqrt{s_{NN}} = 5.02$  TeV. As the production or the yield distribution of the  $X(3915)$  as functions of transverse momenta is dependent on its constituents, it is essential to understand as a first step their transverse momentum distributions in heavy ion collisions, especially at  $\sqrt{s_{NN}} = 5.02$  TeV before calculating the yield or the transverse momentum distribution of the  $X(3915)$ .

If the  $X(3915)$  is in a two- or four-quark state, the  $X(3915)$  meson can be regarded to be produced directly from charm and strange quarks during the quark-hadron phase transition, thereby it is necessary to know the

transverse momentum distribution of charm and strange quarks in the quark-gluon plasma. On the other hand, if the  $X(3915)$  is in a hadronic molecular state, the information on the transverse momentum distribution of the  $D_s$  and  $\bar{D}_s$  mesons is required.

In order to describe the production of the  $X(3915)$  in two- and four-quark states, we adopt here the transverse momentum distributions of charm and strange quarks at mid-rapidities in central collisions obtained from the analysis on the production of  $\phi$  and  $D^0$  mesons at  $\sqrt{s_{NN}} = 5.02$  TeV in relativistic heavy ion collisions [39],

$$\frac{d^2 N_c}{d^2 \vec{p}_{cT}} = \begin{cases} 1.63 (\text{GeV}^{-2}) e^{-0.27(p_{cT}/p_{0T})^{2.03}}, & p_{cT} \leq 1.80 \text{ GeV} \\ 7.95 (\text{GeV}^{-2}) e^{-3.49(p_{cT}/p_{0T})^{3.59}} + \frac{90112 (\text{GeV}^{-2})}{(1.0 + (p_{cT}/p_{0T})^{0.50})^{14.19}}, & p_{cT} > 1.80 \text{ GeV} \end{cases} \quad (33)$$

and

$$\frac{d^2 N_s}{d^2 \vec{p}_{sT}} = \begin{cases} \frac{V}{(2\pi)^3} m_T e^{-m_T/T_{eff}}, & p_{sT} \leq 1.50 \text{ GeV} \\ 21.95 (\text{GeV}^{-2}) e^{-0.17(p_{sT}/p_{0T})^{3.23}} + \frac{80112 (\text{GeV}^{-2})}{(1.0 + (p_{sT}/p_{0T})^{0.65})^{10.29}}, & p_{sT} > 1.50 \text{ GeV} \end{cases} \quad (34)$$

In Eq. (34),  $g_s$ ,  $m_T = \sqrt{p_T^2 + m^2}$ ,  $V$  and  $T_{eff}$  are the degeneracy factor for the color and spin of strange quarks, the transverse mass, the coalescence volume and the effective temperature, respectively. The coalescence volume of  $3360 \text{ fm}^3$  and the effective temperature of  $T_{eff}=173 \text{ MeV}$  have also been applied here [39]. The  $p_{0T}$  in Eq. (34) is taken as  $1.0 \text{ GeV}$  to make the arguments in the transverse momentum distributions dimensionless.

In order to calculate the transverse momentum distribution of the  $X(3915)$  meson in  $D_s \bar{D}_s$  hadronic molecular states, we adopt here the result on the analysis of the  $D_s$  meson production, or the transverse momentum distribution of the  $D_s$  meson evaluated from the above charm and strange quark transverse momentum distributions [39]. However, we consider here two transverse momentum distributions of the  $D_s$  meson; the one at chemical freeze-out and the other at kinetic freeze-out.

It is certain that the hadronic molecular states are formed after their constituents are produced at chemical freeze-out in heavy ion collisions, but it is still uncertain exactly when they are formed from their constituents between chemical and kinetic freeze-outs in heavy ion collisions. In one extreme case, it is possible for them to be produced right after their constituents are produced at chemical freeze-out. In the other extreme case, they can be produced at kinetic freeze-out after some interactions between their constituents and light hadrons during the hadronic stage. In between two cases, it is also possible that they are produced anytime between chemical and kinetic freeze-outs.

Moreover, as hadrons in molecular states are mostly loosely bound, they may be easily dissociated by light hadrons during the hadronic stage. Thus, when those

hadrons are produced either at chemical freeze-out or anytime between two freeze-outs, their yields are inevitably affected from their interactions between hadrons until kinetic freeze-out, and therefore it is required to investigate the hadronic effects on the production or dissociation of hadrons in molecular states [40–42]. The yield, or the transverse momentum distributions of hadrons in molecular states must be strongly dependent on when they are formed in heavy ion collisions.

By this reason, we present here the yields and transverse momentum distributions for two possibilities in the formation of the  $X(3915)$  meson from  $D_s$  and  $\bar{D}_s$  mesons in heavy ion collisions. At first, we consider the formation of the  $X(3915)$  at chemical freeze-out from  $D_s$  and  $\bar{D}_s$  mesons also produced at chemical freeze-out based on the transverse momentum distribution of  $D_s$  and  $\bar{D}_s$  mesons evaluated in the coalescence model [39]. In this case, the additional production of  $D_s$  and  $\bar{D}_s$  mesons from feed-down contributions are overlooked due to a short time for heavier charm-strange mesons to decay into  $D_s$  mesons before the  $X(3915)$  is formed.

At second, we adopt the transverse momentum distribution of  $D_s$  and  $\bar{D}_s$  mesons after considering the feed-down from heavier charm-strange mesons, or  $D_s^*$ ,  $D_{s0}^*(2317)$ , and  $D_{s1}(2460)$  mesons, also calculated in the coalescence model in order to take into account the formation of the  $X(3915)$  at kinetic freeze-out [39]: the yield and transverse momentum distribution of  $D_s$  mesons evaluated in the coalescence model including feed-down contributions is shown to agree reasonably well with the measurement by ALICE Collaboration [39]. We show in Fig. 1 the transverse momentum distributions of  $D_s$  mesons with and without feed-down contributions.

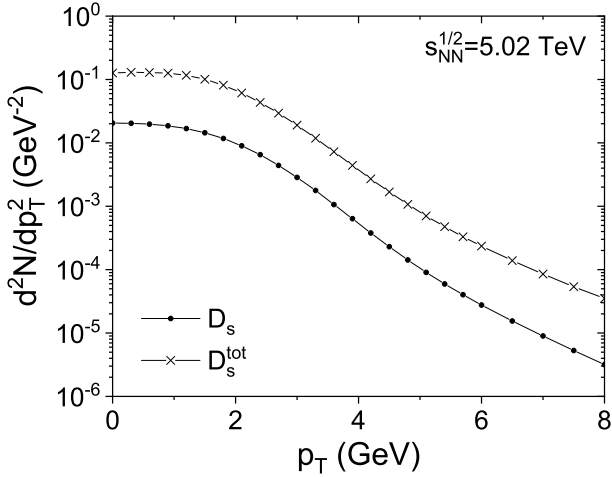


FIG. 1. Transverse momentum distributions of the  $D_s$  meson,  $dN_{D_s}/dp_T$  at mid-rapidity at  $\sqrt{s_{NN}} = 5.02$  TeV with and without feed down contributions, denoted by  $D_s$  and  $D_s^{\text{tot}}$ , respectively.

With the above transverse momentum distribution of  $D_s$  mesons shown in Fig. 1 as well as those of charm and strange quarks, in Eq. (34), we can calculate the transverse momentum distribution of the  $X(3915)$  meson for a hadronic molecular state, a tetraquark state, and a charmonium state. We take the coalescence volume of  $3360 \text{ fm}^3$  [39] for the  $X(3915)$  in a tetraquark or a charmonium state, and a hadronic molecular state produced from bare  $D_s$  mesons at chemical freeze-out, while we adopt the volume at kinetic freeze-out,  $52700 \text{ fm}^3$  determined by requiring both the constant number of light particles and conserving entropy per particle during the hadronic stage [43] in order to describe the production of the  $X(3915)$  at kinetic freeze-out.

We show in Fig. 2(a) transverse momentum distributions of the  $X(3915)$  meson,  $dN_{X(3915)}/dp_T$  at mid-rapidity in central collisions at  $\sqrt{s_{NN}} = 5.02$  TeV for its possible states, or a charmonium state,  $X_{c\bar{c}}$ , a tetraquark state,  $X_{c\bar{c}ss\bar{s}}$ , and a hadronic molecular state formed from  $D_s$  mesons at chemical freeze-out,  $X_{D_s\bar{D}_s}$ , and a hadronic molecular state formed from  $D_s$  mesons at kinetic freeze-out,  $X_{D_s^{\text{tot}}\bar{D}_s^{\text{tot}}}$ . As shown in the Fig. 2(a) the transverse momentum distribution of the  $X(3915)$  in a normal charmonium state is highest, and that of the  $X(3915)$  in a hadronic molecular state formed from  $D_s$  and  $\bar{D}_s$  mesons at kinetic freeze-out is next highest. Two transverse momentum distribution of the  $X(3915)$  both in a tetraquark state and in a hadronic molecular state formed from  $D_s\bar{D}_s$  at chemical freeze-out are found to be very similar.

We note that the formation of the  $X(3915)$  from  $D_s$  and  $\bar{D}_s$  mesons at chemical freeze-out without feed-down contributions is almost the same as the production of the

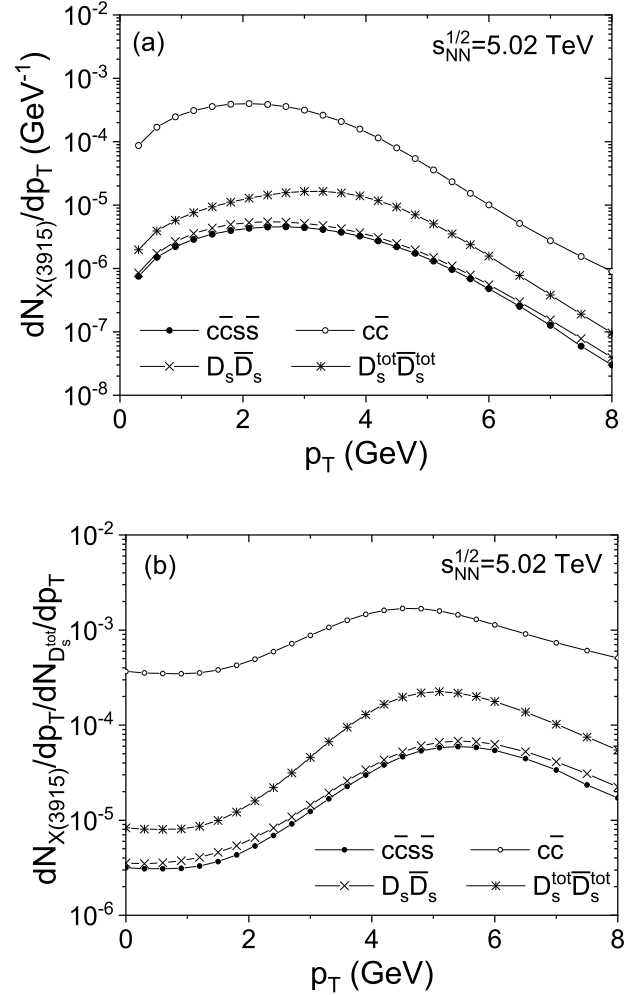


FIG. 2. (a) Transverse momentum distributions of the  $X(3915)$  meson,  $dN_{X(3915)}/dp_T$  at mid-rapidity at  $\sqrt{s_{NN}} = 5.02$  TeV for various possible states, or a charmonium state,  $c\bar{c}$ , a tetraquark state,  $c\bar{c}ss\bar{s}$ , a hadronic molecular state formed from  $D_s$  mesons at chemical freeze-out,  $D_s\bar{D}_s$ , and a hadronic molecular state formed from  $D_s$  mesons at kinetic freeze-out,  $D_s^{\text{tot}}\bar{D}_s^{\text{tot}}$ . (b) Transverse momentum distribution ratios between the  $X(3915)$  of various states and the  $D_s$  meson.

$X(3915)$  in a tetraquark state when  $c\bar{s}$  and  $\bar{c}s$  are formed first, followed by  $c\bar{c}ss\bar{s}$  formation, based on the following relative coordinates,

$$\vec{R} = \frac{m_s \vec{r}_s + m_{\bar{s}} \vec{r}_{\bar{s}} + m_c \vec{r}_c + m_{\bar{c}} \vec{r}_{\bar{c}}}{m_s + m_{\bar{s}} + m_c + m_{\bar{c}}},$$

$$\vec{r}_1 = \vec{r}_c - \vec{r}_{\bar{s}},$$

$$\vec{r}_2 = \vec{r}_{\bar{c}} - \vec{r}_s,$$

$$\vec{r}_3 = \frac{m_c \vec{r}_c + m_{\bar{s}} \vec{r}_{\bar{s}}}{m_c + m_{\bar{s}}} - \frac{m_{\bar{c}} \vec{r}_{\bar{c}} + m_s \vec{r}_s}{m_{\bar{c}} + m_s}, \quad (35)$$

and corresponding relative transverse momenta,

$$\begin{aligned}
\vec{k} &= \vec{p}'_{sT} + \vec{p}'_{\bar{s}T} + \vec{p}'_{cT} + \vec{p}'_{\bar{c}T}, \\
\vec{k}_1 &= \frac{m_{\bar{s}}\vec{p}'_{cT} - m_c\vec{p}'_{\bar{c}T}}{m_c + m_{\bar{s}}}, \\
\vec{k}_2 &= \frac{m_s\vec{p}'_{\bar{c}T} - m_{\bar{c}}\vec{p}'_{sT}}{m_{\bar{c}} + m_s}, \\
\vec{k}_3 &= \frac{(m_{\bar{c}} + m_s)(\vec{p}'_{cT} + \vec{p}'_{\bar{s}T}) - (m_c + m_{\bar{s}})(\vec{p}'_{\bar{c}T} + \vec{p}'_{sT})}{m_s + m_{\bar{s}} + m_c + m_{\bar{c}}}.
\end{aligned} \tag{36}$$

As mentioned before, the yield or transverse momentum distribution of the hadron in a tetraquark state is independent of different configurations between quarks for their relative coordinates and momenta, either Eqs. (26) and (27) or Eqs. (35) and (36) on the condition that all quarks are in  $s$ -wave states, suitable for the  $s$ -wave Gaussian Wigner function with a common oscillator frequency  $\omega$  [38]. Thus, it is possible that the transverse momentum distribution of the  $X(3915)$  in a hadronic molecular state formed from  $D_s$  and  $\bar{D}_s$  mesons at chemical freeze-out can be almost same as that of the  $X(3915)$  in a tetraquark state. In that sense the yield or transverse momentum distributions of the exotic hadrons in a multiquark state can play a role as a limiting values for those of exotic hadrons in a hadronic molecular state.

However, here in the case of the formation of the  $X(3915)$  in a hadronic molecular state, the different oscillator frequency  $\omega=0.0876$  GeV, representing for the loose binding between  $D_s$  and  $\bar{D}_s$  mesons, has been adopted, thereby making the above two transverse momentum distributions little bit different. On the other hand, the transverse momentum distribution of the  $X(3915)$  in a hadronic molecular state produced at kinetic freeze-out is evaluated to be about three times larger than that of the  $X(3915)$  produced at chemical freeze-out. The difference between the transverse momentum distributions of the  $X(3915)$  in a harmonic molecular state at chemical and kinetic freeze-outs is attributable to both the larger number of  $D_s$  mesons at kinetic freeze-out due to feed-down contributions and the larger freeze-out volume, compared to the number of  $D_s$  mesons with the coalescence volume at chemical freeze-out; the number of  $D_s$  mesons increases by 6.8 times while the volume of the system increases by about 15.7 times between chemical and kinetic freeze-out, thereby resulting in  $6.8^2/15.7 \approx 2.9$ .

The different behaviors of transverse momentum distribution of the  $X(3915)$  meson in various possible states are shown more explicitly when the ratios of the transverse momentum distribution between the  $X(3915)$  of those states and the  $D_s$  meson are taken. Moreover, when the decay of the  $X(3915)$  meson to  $D_s$  and  $\bar{D}_s$  mesons has been considered [10], the measurement of the ratio between the  $X(3915)$  and  $D_s$  meson is expected to reduce experimental uncertainties in the observation of the  $X(3915)$ .

We show in Fig. 2(b) transverse momentum distribution ratios between the  $X(3915)$  of various states and the

TABLE IV. Yields of the  $X(3915)$  for various possible states evaluated from the integration of the transverse momentum distributions shown in Fig. 2(a) over all transverse momenta at  $\sqrt{s_{NN}} = 5.02$  TeV at LHC. The yield of the  $X(3915)$  in a thermal model [39] is also listed for comparison.

	$c\bar{c}$	$c\bar{c}s\bar{s}$	$D_s\bar{D}_s$	$D_s^{tot}\bar{D}_s^{tot}$	Ther.
Yields ( $\times 10^{-4}$ )	12.0	0.162	0.194	0.567	6.38

$D_s$  meson. As shown in Fig. 2(b), all the ratios increase with increasing transverse momenta at low  $p_T$ , and have the peak at the intermediate transverse momentum regions. The ratio between the  $X(3915)$  in a molecular state produced at kinetic freeze-out and the  $D_s$  meson increases by about 20 times in the intermediate transverse momentum regions, while the ratio between the  $X(3915)$  in a charmonium state and the  $D_s$  meson increases by about 2 times, showing different behaviors in the ratios between the  $X(3915)$  and the  $D_s$  depending on the structure of the  $X(3915)$ .

Integrating transverse momentum distributions of the  $X(3915)$  meson in its various states over the entire transverse momentum region leads to their yields, and the results are shown in Table IV. Also listed in Table IV is the yield of the  $X(3915)$  evaluated in a thermal model [39] for comparison. As argued on the transverse momentum distribution of the  $X(3915)$  before, the yield of the  $X(3915)$  in a  $D_s\bar{D}_s$  state is also calculated to be slightly larger than the yield of the  $X(3915)$  in a  $c\bar{c}s\bar{s}$  state, and the yield of the  $X(3915)$  in a  $D_s^{tot}\bar{D}_s^{tot}$  state at kinetic freeze-out is about three times larger than that of the  $X(3915)$  in a  $D_s\bar{D}_s$  state at chemical freeze-out.

The yield of the  $X(3915)$  in a charmonium state is found to be larger by about a factor of two compared to that in a thermal model. Considering the constituent mass of charm quarks, 1500 MeV, one can expect that the yield of the  $X(3915)$  in a  $c\bar{c}$  state is closer to that of the  $J/\psi$  meson, thereby larger than the yield of the  $X(3915)$  in a thermal model due to its mass 3922.1 MeV. Even though the production of the  $X(3915)$  is suppressed owing to the internal relative momentum, the  $2p$ -wave, the yield of the  $X(3915)$  in a charmonium state is found to be still larger than the expectation from the thermal model.

On the other hand, the yield of the  $X(3915)$  in a compact tetraquark state is evaluated to be smaller by about a factor of forty compared to that in a thermal model, supporting the scenario for the suppressed production of the multiquark hadrons by coalescence in heavy ion collisions [20–22]. Moreover, it is worthwhile to note that the yield of the  $X(3915)$  in a hadronic molecular state is also calculated to be smaller than that in a thermal model, different from most exotic hadrons except the  $D_{s0}^*(2317)$ , another charm-strange meson [20–22].

Therefore, together with the transverse momentum

distributions of the  $X(3915)$  meson as shown in Fig. 2, it is expected that the yield of the  $X(3915)$  meson for proposed states in Table IV would be helpful in specifying the internal structure of the  $X(3915)$  meson among its proposed states from the measurement of its production in heavy ion collisions.

## VI. CONCLUSIONS

We have investigated the  $X(3915)$  as a  $c\bar{c}s\bar{s}$  state in a quark model and studied its production in heavy ion collisions using a coalescence model. Within the quark model, we analyze the internal color-spin structure of the  $X(3915)$  together with its spatial wave function and find that the dominant component of the ground state corresponds to a well separated  $D_s\bar{D}_s$  configuration. This result suggests that the  $X(3915)$  more likely corresponds to a hadronic molecular state, dominated by long range interactions beyond the description of the quark model. Nevertheless, given the uncertainties of the quark model, a compact tetraquark configuration cannot be conclusively ruled out.

Along with the analysis on the quark model, we have also studied the production of the  $X(3915)$  meson, focusing on its production by coalescence in relativistic heavy ion collisions at  $\sqrt{s_{NN}} = 5.02$  TeV at LHC. Considering three proposed states for the  $X(3915)$ —a charmonium, a tetraquark, and a hadronic molecular state—we have evaluated the yields and transverse momentum distributions of the  $X(3915)$  for each state, and have investigated the possibilities of its production in heavy ion collisions. Moreover, we have considered two scenarios for the  $X(3915)$  in a hadronic molecular state, produced at both chemical and kinetic freeze-outs.

The yield of the  $X(3915)$  in a charmonium state is found to be larger compared to those of the  $X(3915)$  in both a hadronic molecular and a tetraquark state, and even larger than the yield in a thermal model by about a factor of two. On the other hand, the yields in both a hadronic molecular state and a tetraquark state are smaller compared to that in a thermal model, reflecting the suppressed production of the multiquark hadrons by coalescence in heavy ion collisions.

We find that the yield of the  $X(3915)$  in a  $D_s\bar{D}_s$  state formed right after  $D_s$  mesons are produced at chemical freeze-out is slightly larger than the yield of the  $X(3915)$  in a  $c\bar{c}s\bar{s}$  state, and the yield of the  $X(3915)$  in a  $D_s^{tot}\bar{D}_s^{tot}$  state at kinetic freeze-out is larger by about a factor of three compared to that of the  $X(3915)$  in a  $D_s\bar{D}_s$  state at chemical freeze-out. It is noticeable to see the smaller yields of the  $X(3915)$  in both a hadronic molecular and a tetraquark state compared to that in a thermal model, similar to the case for the  $D_{s0}^*(2317)$  meson.

Therefore, investigating the  $X(3915)$  meson based on both the quark model and its production in heavy ion collisions presents us with chances to understand the structure of the  $X(3915)$  in more detail. We expect that the observation of the  $X(3915)$  meson in relativistic heavy ion collisions would help identify the internal structure of the  $X(3915)$  meson in the near future.

## ACKNOWLEDGEMENTS

This work was supported by the National Research Foundation of Korea (NRF) grant funded by the Korea government (MSIT) No. RS-2023-00280831, No. RS-2025-23963552, No. 2023R1A2C300302311 and No. 2023K2A9A1A0609492411.

---

[1] S. K. Choi *et al.* (Belle Collaboration), Phys. Rev. Lett. **91**, 262001 (2003).  
[2] A. Esposito, A. Pilloni and A. D. Polosa, Phys. Rept. **668**, 1-97 (2017).  
[3] N. Brambilla, S. Eidelman, C. Hanhart, A. Nefediev, C. P. Shen, C. E. Thomas, A. Vairo and C. Z. Yuan, Phys. Rept. **873**, 1-154 (2020).  
[4] H. X. Chen, W. Chen, X. Liu, Y. R. Liu and S. L. Zhu, Rept. Prog. Phys. **86**, no.2, 026201 (2023).  
[5] K. Abe *et al.* (Belle Collaboration), Phys. Rev. Lett. **94**, 182002 (2005).  
[6] B. Aubert *et al.* (BaBar Collaboration), Phys. Rev. Lett. **101**, 082001 (2008).  
[7] P. del Amo Sanchez *et al.* (BaBar Collaboration), Phys. Rev. D **82**, 011101 (2010).  
[8] S. Uehara *et al.* (Belle Collaboration), Phys. Rev. Lett. **104**, 092001 (2010).  
[9] J. P. Lees *et al.* (BaBar Collaboration), Phys. Rev. D **86**, 072002 (2012).  
[10] S. Navas *et al.* (Particle Data Group Collaboration), Phys. Rev. D **110**, no.3, 030001 (2024).  
[11] R. Aaij *et al.* (LHCb Collaboration), Phys. Rev. Lett. **131**, no.7, 071901 (2023).  
[12] X. Li and M. B. Voloshin, Phys. Rev. D **91**, no.11, 114014 (2015).  
[13] R. F. Lebed and A. D. Polosa, Phys. Rev. D **93**, no.9, 094024 (2016).  
[14] M. X. Duan, S. Q. Luo, X. Liu and T. Matsuki, Phys. Rev. D **101**, no.5, 054029 (2020).  
[15] P. G. Ortega, J. Segovia, D. R. Entem and F. Fernández, Phys. Lett. B **778**, 1-5 (2018).  
[16] M. Suzuki, Phys. Rev. D **72**, 114013 (2005).  
[17] Y. Dong, A. Faessler, T. Gutsche, S. Kovalenko and V. E. Lyubovitskij, Phys. Rev. D **79**, 094013 (2009).  
[18] M. Takizawa and S. Takeuchi, PTEP **2013**, 093D01 (2013).  
[19] H. Yun, D. Park, S. Noh, A. Park, W. Park, S. Cho, J. Hong, Y. Kim, S. Lim and S. H. Lee, Phys. Rev. C **107**, no.1, 014906 (2023).  
[20] S. Cho *et al.* (ExHIC Collaboration), Phys. Rev. Lett. **106**, 212001 (2011).

- [21] S. Cho *et al.* (ExHIC Collaboration), Phys. Rev. C **84**, 064910 (2011).
- [22] S. Cho *et al.* (ExHIC Collaboration), Prog. Part. Nucl. Phys. **95**, 279 (2017).
- [23] W. Park, S. Noh and S. H. Lee, Nucl. Phys. A **983**, 1-19 (2019).
- [24] S. Noh, W. Park and S. H. Lee, Phys. Rev. D **103**, 114009 (2021).
- [25] S. Noh and W. Park, Phys. Rev. D **108**, no.1, 014004 (2023).
- [26] W. Park and S. Noh, Phys. Rev. D **110**, no.7, 074041 (2024).
- [27] J. Wu, Y. R. Liu, K. Chen, X. Liu and S. L. Zhu, Phys. Rev. D **94**, no.9, 094031 (2016).
- [28] F. X. Liu, R. H. Ni, X. H. Zhong and Q. Zhao, Eur. Phys. J. C **85**, no.11, 1303 (2025).
- [29] F. K. Guo and U. G. Meissner, Phys. Rev. D **86**, 091501 (2012).
- [30] S. L. Olsen, Phys. Rev. D **91**, no.5, 057501 (2015).
- [31] V. Greco, C. M. Ko, and P. Levai, Phys. Rev. Lett. **90**, 202302 (2003).
- [32] V. Greco, C. M. Ko, and P. Levai, Phys. Rev. C **68**, 034904 (2003).
- [33] S. Cho, Phys. Rev. C **91**, no. 5, 054914 (2015).
- [34] S. Cho, Phys. Rev. C **109**, no.5, 054904 (2024).
- [35] Y. Oh, C. M. Ko, S. H. Lee, and S. Yasui, Phys. Rev. C **79**, 044905 (2009).
- [36] R. Scheibl and U. W. Heinz, Phys. Rev. C **59**, 1585 (1999).
- [37] M. Kordell, II, R. J. Fries and C. M. Ko, Annals Phys. **443**, 168960 (2022).
- [38] S. Cho and S. H. Lee, Phys. Rev. C **101**, no. 2, 024902 (2020).
- [39] S. Cho and S. H. Lee, arXiv:2510.18673.
- [40] S. Cho and S. H. Lee, Phys. Rev. C **88**, 054901 (2013).
- [41] A. Martinez Torres, K. P. Khemchandani, F. S. Navarra, M. Nielsen and L. M. Abreu, Phys. Rev. D **90**, no. 11, 114023 (2014).
- [42] J. Hong, S. Cho, T. Song and S. H. Lee, Phys. Rev. C **98**, no.1, 014913 (2018).
- [43] H. S. Sung, S. Cho, J. Hong, S. H. Lee, S. Lim and T. Song, Phys. Lett. B **819**, 136388 (2021).